Evolution of the interfacial phases in Al_2O_3–Kovar® joints brazed using a Ag–Cu–Ti-based alloy

Majed Ali[a,*], Kevin M. Knowles[a], Phillip M. Mallinson[b], John A. Fernie[b]

[a]*Department of Materials Science and Metallurgy, University of Cambridge, 27 Charles Babbage Road, Cambridge, CB3 0FS, UK*
[b]*AWE plc, Aldermaston, Reading, Berkshire, RG7 4PR, UK*

Abstract

A systematic investigation of the brazing of Al_2O_3 to Kovar® (Fe–29Ni–17Co wt.%) using the active braze alloy (ABA) Ag–35.25Cu–1.75Ti wt.% has been undertaken to study the chemical reactions at the interfaces of the joints. The extent to which silica-based secondary phases in the Al_2O_3 participate in the reactions at the ABA/Al_2O_3 interface has been clarified. Another aspect of this work has been to determine the influence of various brazing parameters, such as the peak temperature, T_p, and time at T_p, τ, on the resultant microstructure. As a consequence, the microstructural evolution of the joints as a function of T_p and τ is discussed in some detail.

The formation of a Fe_2Ti layer on the Kovar® and its growth, along with adjacent Ni_3Ti particles in the ABA, dominate the microstructural developments at the ABA/Kovar® interface. The presence of Kovar® next to the ABA does not change the intrinsic chemical reactions occurring at the ABA/Al_2O_3 interface. However, the extent of these reactions is limited if the purity of the Al_2O_3 is high, and so it is necessary to have some silica-rich secondary phase in the Al_2O_3 to facilitate the formation of a Ti_3Cu_3O layer on the Al_2O_3. Breakdown of the Ti_3Cu_3O layer, together with fracture of the Fe_2Ti layer and separation of this layer from the Kovar®, has been avoided by brazing at temperatures close to the liquidus temperature of the ABA for short periods of time, e.g. for T_p between 820 and 830 °C and τ between 2 and 8 min.

Keywords: Brazing, Joining, Alumina, Al_2O_3, Kovar, Cusil ABA.

* Corresponding author.
E-mail address: ma591@cam.ac.uk (M. Ali).

1. Introduction

Alumina is widely used in the electronics, refractory ceramics and automotive industries [1]. A connection to a metal is often required in a number of applications for this ceramic. An example of such a connection can be found in a spark plug, where a steel casing is shrink-fitted around the alumina [2]. Other feedthrough assemblies, such as those used in sensors to measure pressures in aircraft systems, require chemically bonded metal–alumina interfaces to produce hermetic bonds.

Joining a ceramic to a metal is particularly difficult. This is because ceramics typically have a significantly lower coefficient of thermal expansion (CTE) than metals. A consequence of the CTE mismatch is the development of stresses near a join, particularly at the free surfaces of the joined components as the joint is cooled from the bonding temperature [3]. In some cases, these stresses can lead to failure of the joint, even with good chemical bonding at the metal/ceramic interface [4]. One method used to help alleviate the effects of a CTE mismatch between the alumina and the metal is to bond the alumina to an intermediate material that has a similar CTE and a lower elastic modulus. An iron-nickel-cobalt alloy with a composition of approximately Fe–29Ni–17Co wt.%, also known commercially as Kovar®, is used in feedthrough devices for the transition between the alumina and metal. The CTE of Kovar® between room temperature and its Curie temperature (T_c) of ~435 °C is ~5.5×10^{-6} K^{-1} [5] (for this range of temperature the CTEs for >85 wt.% α−Al_2O_3-based ceramics vary between ~5.5 and ~9.0×10^{-6} K^{-1} [6]). There is a discontinuous change in the CTE of Kovar® to a noticeably higher value for temperatures above its T_c [5]. The thermally-induced stresses in an alumina–Kovar® joint can sometimes be accommodated by using eutectic Ag–28Cu wt.%-based braze alloys to achieve a bond [7].

Active metal brazing is a relatively simple technique to join alumina to a metal or to itself. In this technique, the braze alloy has a small quantity of an element added so that it can react with the alumina to form compounds at the braze/alumina interface to enable the liquid braze to spread over the ceramic surface. The added element is known as an active element and the braze alloy is called an active braze alloy (ABA). As a consequence, a processing step to modify the bonding surface of the alumina chemically to make it more wettable by a conventional braze alloy, such as the Ag–Cu

eutectic alloy, is avoided. Such a process can involve several complex steps to achieve a suitable 'metallised' surface on the alumina; the sintered metal powder process known as the moly–manganese process is an example [8,9].

In the literature, active metal brazing of alumina to Kovar® has typically been reported using Ag–Cu eutectic or near–eutectic alloys with added Ti as the active element, at a level of about 1.5–5 wt.%. The chemical reactions that occur between Al_2O_3 and two Ag–Cu–Ti-based ABAs with quantities of Ti in this range, known by their trade names of Cusil ABA® (Ag–35.25Cu–1.75Ti wt.%) and Ticusil® (Ag–26.7Cu–4.5Ti wt.%), have recently been investigated in some detail [10]. A typical brazing procedure to join ≥95 wt.% Al_2O_3 to itself using these two ABAs results in a metastable layered structure at the Ag–Cu–Ti/Al_2O_3 interface that is primarily comprised of Ti_3Cu_3O, which is in contact with the ABA, alongside a thin γ-TiO layer on the Al_2O_3 [11]. By comparison with what is now known about this interface, there is a lack of detailed knowledge about the chemical processes at the ABA/Al_2O_3 interface in Al_2O_3–Kovar® joints brazed with Ag–Cu–Ti-based ABAs. This is partly because during brazing the chemical elements in the Kovar® react immediately with the Ti in the ABA. As a consequence, this limits the amount of reaction product(s) formed at the Ag–Cu–Ti/Al_2O_3 interface. Either a thin reaction layer, typically ≤1 μm in width, or small individual particles are found at this latter interface. Therefore, it is difficult to analyse the interfacial phase(s) for their crystal structure or composition using techniques such as X-ray diffraction (XRD) or energy-dispersive X-ray spectroscopy (EDS) in a scanning electron microscope (SEM).

The work of Stephens et al. [12–14] indicates that it is essential to have a continuous reaction layer at both the Ag–Cu–Ti/Al_2O_3 interface and the Ag–Cu–Ti/Kovar® interface to form hermetic Al_2O_3–Kovar® joints. In their work, the phase that forms at this interface is referred to as Ti_xO_y, although no conclusive experimental evidence was reported to suggest it is indeed a titanium oxide. Schilm et al. [15] have observed a 0.7–1 μm thick continuous layer on 96 wt.% Al_2O_3 after joining to Kovar® using a 50 μm thick Cusil ABA® foil and a brazing cycle that peaked at 830 °C for 10 min. The precise chemical composition of this layer is not given, but it is reported to contain Ti and O, along with small quantities of Fe, Ni and Co from the Kovar®. The

composition of a reaction layer that formed on the Al_2O_3 in a joint which was held at 850 °C for 10 min has been reported to be 36.6Ti–25.0Ni–12.6Fe–4.7Co–4.3Cu–4.1Al–12.5O–1.3Ag wt.% (note there is an error in this composition because the total percentage by mass exceeds 100%). Wang et al. [16] also have measured significant quantities of elements from the Kovar®, particularly Ni and Fe, in a continuous 1–2 μm thick reaction layer. This layer formed on 95 wt.% Al_2O_3 which was joined to Kovar® using a 100 μm thick Cusil ABA® foil and with a brazing cycle that peaked at 900 °C for 5 min. The formation of a particularly thick layer can be attributed to brazing at a high peak temperature with a thicker ABA. Wang et al. [16] suggest that this reaction layer is TiO based on its chemical composition of 38.8Ti–15.5Ni–8.9Fe–2.8Co–5.5Cu–6.9Al–18.0O–2.2Si at.% and XRD data collected from the Ag–Cu–Ti/Al_2O_3 interface. It is anticipated that the reaction layer itself contains significant quantities of the elements from the Kovar®, particularly Ni and Fe, because the quantities of these elements in the phases such as Al_2O_3, Ag and Cu surrounding the reaction layer are expected to be low. Furthermore, there is no evidence of another phase containing the chemical elements of the Kovar® next to the reaction layer. These observations suggest that either a titanium oxide is forming on the Al_2O_3 that can accommodate considerable quantities of Ni and Fe or a more chemically complex phase is produced.

A reaction layer on the Al_2O_3 was absent in a braze joint that was prepared at a higher temperature of 940 °C by Wang et al. [16]. Instead, large individual Fe_2Ti particles were observed next to the Al_2O_3. This change in the interfacial structure has been explained qualitatively by Wang et al. [16] in terms of the residual amount of Ti in the ABA available to react with the Al_2O_3 after the Ti had first reacted with some of the elements in the Kovar® which had dissolved into the liquid ABA, forming various intermetallic compounds such as Fe_2Ti and Ni_3Ti. The same explanation for the absence of a continuous reaction layer on the Al_2O_3 was first introduced by Stephens et al. [12–14] as a Ti scavenging process, in which the chemical reactions between the ABA and the Kovar® in the initial stages of brazing prevent Ti from diffusing to, and reacting with, the Al_2O_3. The Ti in the ABA should diffuse to both interfaces of the joint after the ABA melts. If the rates of the chemical reactions at the ABA/Kovar® interface are significantly higher than those occurring at the ABA/Al_2O_3 interface, a

significant proportion of the Ti could indeed be consumed to form various intermetallic compounds at the ABA/Kovar® interface before a continuous layer on the Al_2O_3 forms. The studies by Stephens et al [12] and Wang et al. [16] suggest a continuous reaction layer on the Al_2O_3 forms before breaking down at the peak brazing temperature, and so it might be possible to control the structure of this layer to some extent by carefully selecting the processing conditions. It is apparent that thermal decomposition of the layer on the Al_2O_3 has not been considered. Clearly, further work is required to identify the phase(s) forming on the Al_2O_3. It would also be worthwhile to investigate the stability of the phase(s) at the peak temperature of a brazing cycle to determine the rate of any significant microstructural changes in a joint, particularly at the Ag–Cu–Ti/Al_2O_3 interface.

Two compounds are usually observed in the ABA of Al_2O_3–Kovar® joints, in the form of a complex chain of small micron-sized particles that extends across the joint [13–18]. EDS, and to a much lesser extent XRD, have been used to identify these compounds as Fe_2Ti and Ni_3Ti. Considerable quantities of Fe and Ni, and also other metals such Co or Cu, are typically incorporated in these compounds. This is probably a result of substitution of the Fe or Ni in the two compounds. The work of Schilm et al. [15] suggests that these compounds form on the Kovar® before separating into the ABA. In their work, a Fe–rich layer was observed directly on Kovar® at a Cusil ABA®/Kovar® interface in a 96 wt.% Al_2O_3–Kovar® joint heated to 830 °C for 10 min. This layer was approximately 2–3 μm thick and also contained Ni, Co and Ti. A much thinner Ni–rich layer containing Co, Fe and Ti was also observed between the Fe–rich layer and the ABA. Individual particles containing Ni, Cu and Ti were also identified in the ABA, and they were either in contact with the Ni–rich layer or close to it. However, conclusive experimental evidence identifying all of the phases at the Ag–Cu–Ti/Kovar® interface has not been found. Consequently the chemical processes at this interface are not fully understood.

Very low hermetic yields were obtained by Stephens et al. [12] for joints made with a Kovar® spacer that was brazed between two pieces of 94 wt.% Al_2O_3 using Cusil ABA®. Brazing was performed at temperatures between 810 and 900 °C for 5 to 10 min and also at 850 °C for up to 30 min. Joints that were identified to have

hermetically sealed interfaces contained a continuous reaction layer on the Al_2O_3. This continuous reaction layer formed in a small selection of joints that were either brazed for 10 min or less at 850 °C or for 5 min at higher temperatures. The microstructures of these particular joints were not reproducible, because a number of joints prepared using these conditions were not hermetic. All other conditions used produced a discontinuous layer on the Al_2O_3. The joints typically failed at a maximum tensile stress between ~35 and ~80 MPa, which was considered to be satisfactory for the particular application. A correlation between the hermiticity and the tensile strengths of the joints was not identified. The investigations by Stephens et al. [12,13] demonstrate that forming hermetically sealed joints using Cusil ABA® is not straightforward. The difficulties experienced by Stephens et al. [19] in fulfilling this very task ultimately motivated them to develop a new ABA that utilises Zr as the active element specifically to join Al_2O_3 to Kovar®. It is particularly apparent from the work of Stephens et al. [12] and Wang et al. [16] that the interfacial microstructure between the ABA and the Al_2O_3 can be controlled to some extent by altering the peak temperature of the brazing cycle (T_p) used or time at T_p (τ). It is evident from the available literature that the effects of altering these two variables on the overall microstructure of joints, and the extent to which they result in significant microstructural developments, have not yet been defined clearly.

In the work reported here, a comprehensive evaluation of several Al_2O_3/Cusil ABA®/Kovar® joints using electron microscopy-based techniques has been undertaken to determine conclusively the interfacial reaction products which form over a wide range of conditions. The microstructural characterisation work has been used ultimately to develop a better understanding of the evolution of the interfacial phases. This is particularly important for the phase(s) forming at the Ag–Cu–Ti/Al_2O_3 interface, because it appears that the interfacial phase(s) can break down at high T_p or by extending τ at a specific T_p. 99.7 and 95 wt.% Al_2O_3 have been used to study the extent to which silica-based secondary phases in the Al_2O_3 participate in the chemical reactions at the ABA/Al_2O_3 interface. All of the joints have been prepared using Cusil ABA®, which is a commercially available Ag–Cu–Ti-based ABA containing a relatively low quantity of Ti. It was anticipated that a limited quantity of Ti would make it less difficult to study the reaction process occurring at the interfaces in the

early stages of brazing. This particular Ag–Cu–Ti-based ABA is also widely used for the brazing of Al_2O_3. The effects of altering processing variables such as T_p and τ on the microstructure of the joints prepared with 95 wt.% Al_2O_3 have also been studied.

2. Experimental

2.1. Materials

Cusil ABA® (Ag–35.25Cu–1.75Ti wt.%) has been used to join Kovar® (Fe–29Ni–17Co wt.%) to 95 and 99.7 wt.% Al_2O_3. The ABA was supplied by VBC Group Ltd (UK) in foil form, with a thickness of ~50 μm, from which 10 × 5 mm sections were taken for joining. SEM investigation of the as-received ABA revealed that the active element, Ti, is in the form of Cu_4Ti particles randomly distributed in a Ag–Cu eutectic alloy [10]. The as-received Kovar® was composed of equiaxed grains of various sizes, ranging from ~10 to ~100 μm in width, which have a face-centered cubic crystal structure with a lattice parameter a = 3.6 Å. No significant changes in the microstructure and the crystal structure of Kovar® were identified after brazing.

Braze joints made with 95 wt.% Al_2O_3 containing silica as the main secondary phase were compared with joints made with high purity 99.7 wt.% Al_2O_3. After polishing and coating with a thin layer of carbon, electron microprobe analysis of the bonding surfaces of these ceramics was performed to determine their composition. A Cameca SX-100 (France) electron microprobe operated at 15 keV with a 10 nA electron beam was used in the wavelength-dispersive mode. Calibration of the elements of interest used several mineral standards. The compositions of the ceramics are given in Table 1. The Si and Ca in the 95 wt.% Al_2O_3 are very likely to be in the form of oxides. EDS and electron diffraction data collected after brazing the 95 wt.% Al_2O_3 to itself shows intergranular SiO_2 present in the ceramic. Al_2O_3 in the form of 10 × 5 × 4 mm plates were brazed to 10 × 5 × 0.5 mm plates of Kovar®. Prior to brazing, all of the components of a joint were cleaned separately in an ultrasonic bath of detergent for up to 15 min.

2.2. Brazing process

Al_2O_3/Cusil ABA®/Kovar® joints were prepared in an atmosphere of purified argon, which was established in a horizontal electric furnace (STF 15/450, Carbolite, UK) as described in [10]. The BIP® technology by Air Products and Chemicals (USA) was used to purify the argon gas entering the furnace. A heating rate of 10 °C min^{-1} was used. The cooling rate was ~20 °C min^{-1} between the peak temperature used and ~500 °C, after which it reduced significantly during a furnace cool to room temperature. A pressure of ~4 kPa was applied to all of the joints using a 20 g weight to improve contact across the components.

The combinations of T_p and τ used to braze the two types of Al_2O_3 to Kovar® are given in Table 2. Brazing of 95 wt.% Al_2O_3 was carried out with T_p ranging from the liquidus temperature of the ABA of 815 °C to 900 °C. For these brazing experiments τ varied between 0 and 45 min. The low quantity of secondary phase in 99.7 wt.% Al_2O_3 made it difficult to establish a bond between the Al_2O_3 and the ABA. Consequently, brazing of this ceramic was carried out to a lesser extent, with T_p ranging from 815 °C to 875 °C and τ ranging from 0 to 45 min, as described in Table 2.

2.3. Analytical processes

A field emission SEM, Leo 1530 VP, Leo Electron Microscopy - Carl Zeiss®, Germany, operated at 20 kV was used to observe the microstructures of joints, before undertaking more detailed examinations of joints by transmission electron microscopy. This microscope was equipped with an energy dispersive spectrometer (INCA-7426, Oxford Instruments®, UK), which was particularly useful to analyse the compositions of the phases next to the Kovar®. Typically, four cross-sections of each joint were analysed with this microscope to monitor the homogeneity of the interfacial structures and chemistry across the joint. A low speed diamond saw was used to cut out cross-sections of joints, which were mounted in acrylic resin at room temperature, polished and then coated with a thin layer of carbon before observations were made. It was necessary to mount all of the joints made with 99.7 wt.% Al_2O_3 in clear resin before cutting out cross-sections, because the Al_2O_3 broke away from the ABA while cutting these joints.

A scanning transmission electron microscope (STEM), Tecnai Osiris™, FEI, USA,

operated at 200 kV was also used to perform elemental analysis using an EDS system (Super-X system, FEI, USA). Data from the transmission electron microscopes (TEMs) used in this work were particularly useful to study the very thin interfacial phases developing on the Al_2O_3. Thin sections of joints were prepared for TEM analysis using a focused ion beam instrument, FIB, (Helios Nanolab™, FEI, USA). The procedure commonly known as the lift-out technique [20] was used to transfer sections of joints up to 25 × 10 μm to molybdenum grids, or a carbon substrate on a molybdenum grid. These sections were subsequently reduced to a thickness of ~100 nm using the FIB.

Selected area diffraction patterns were collected to determine the crystal structures of phases using a conventional TEM (200CX, JEOL®, Japan), which was operated at 200 kV. The camera length of this microscope was monitored at regular intervals using an Al thin film, which was supplied by Agar Scientific, UK.

The thicknesses of the reaction layers were measured as a function of T_p and τ from images collected using the SEM; a mean value and ± one standard deviation from twenty measurements are reported.

3. Results

3.1. Brazing 95 wt.% Al_2O_3 to Kovar®

Subtle and progressive changes in the microstructure of joints between 95 wt.% Al_2O_3 and Kovar® were observed, particularly as a function of τ. Therefore, the microstructural developments at each T_p used are discussed separately as a function of τ.

3.1.1. Brazing 95 wt.% Al_2O_3 at 815 °C

Back-scattered electron images (BSEIs) of cross-sections of 95 wt.% Al_2O_3–Kovar® joints that were held at 815 °C for 0 to 45 min are shown in Figures 1 and 2. Heating a joint to 815 °C and then maintaining this temperature for a nominal 1 s before cooling is not sufficient to bond the ABA chemically to the Al_2O_3. When the ABA melts, the Kovar® immediately reacts with it to form a continuous layer that is about 1.3 μm thick at the ABA/Kovar® interface, as shown in Figure 1a. EDS analysis of this layer

indicated that it is Fe-rich with a typical mean composition of 42Fe–34Ti–11Co–9Ni–4Cu at.%. It was also apparent that there were significant variations in the relative amounts of the elements identified in this layer. The amount of Ti varied between 28 and 35 at.%, which are values that approximately describe the range of compositions for non-stoichiometric Fe_2Ti at ~815 °C according to various Fe–Ti phase diagrams [21,22]. A variation of up to ~10 at.% Fe appeared together with variations in the amounts of Ni, Co or Cu to provide a M:Ti ratio, where M is Fe+Co+Ni+Cu, between 1.9 and 2.6. This variation in composition was not dependent on the distance away from the surface of the Kovar® at which measurements were taken. It is apparent that a significant amount of Fe in this layer is substituted by other transition metals such as Ni, Co and Cu in such a way that a variation in the composition across this layer is complex. As a consequence, it was not possible to obtain experimental evidence for the diffusion of elements across this layer.

This Fe-rich layer on the Kovar® is comprised of crystals which have the same structure as Fe_2Ti (hexagonal, $P6_3/mmc$, space group 194) with the lattice parameters a = 4.8 Å and c = 7.8 Å. A selection of indexed electron diffraction patterns from these crystals is shown in Figure 3. The diffraction patterns indicate that this layer forms by a chemical reaction between the Kovar® and the ABA to produce a solid solution of Ni, Co and Cu in Fe_2Ti, by substitution of Fe, rather than forming only by the diffusion of elements in the ABA into the Kovar®. The composition of this layer measured by EDS is consistent with the current estimations of the solubility of Co, Ni and Cu in Fe_2Ti at T_p. Between 800 and 900 °C, Fe_2Ti can accommodate ~35 at.% Co and ~20 at.% Ni [23,24]. The solubility of Cu in Fe_2Ti is significantly lower, approximately 3 at.% at 849 °C [25]. Although an accurate descriptor of this layer could be $(Fe+Co+Ni+Cu)_2Ti$, it is referred to as Fe_2Ti in the text and figures for simplicity.

Small particles, up to 100 nm in diameter, were identified in the Fe_2Ti layer both at grain boundaries and within the Fe_2Ti grains. An annular dark-field image of a ABA/Kovar® interface showing these particles as dark spots in the Fe_2Ti layer, because they have a lower average atomic number than Fe_2Ti, is given in Figure 4, along with the results of EDS area scans containing some of these particles. The EDS measurements indicate that these particles contain Ti. This is consistent with electron

diffraction data which identify the crystal structure of these particles as that of α-Ti (hexagonal, $P6_3/mmc$, space group 194) with the lattice parameters a = 2.9 Å and c = 4.8 Å; a selection of indexed electron diffraction patterns is also shown in Figure 4.

There are three different phases in the form of individual particles that appear to nucleate on the Fe_2Ti layer. One of these phases is typically observed as a number of very small particles forming a thin broken layer directly on the Fe_2Ti layer (Figure 1a). This phase has a lower average atomic number than Fe_2Ti, and so it appears darker than the Fe_2Ti layer in the BSEIs shown in Figure 1a. The composition of this phase was measured by EDS in the STEM, typically as 46Ti–20Fe–16Ni–11Co–6Cu–1Al at.%. Its crystal structure was identified as that of FeTi (cubic, $Pm\bar{3}m$, space group 221, a = 2.9 Å), which is isostructural with CoTi and also a high temperature form of NiTi [26,27]. A selection of indexed electron diffraction patterns from this phase is shown in Figure 5. Extensive substitution of Fe by other similar-sized transition metals such as Ni, Co and Cu also occurs in this phase. This is because FeTi can accommodate a significant amount of Cu at T_p, approximately ~ 35 at.% at 849 °C [25], and it forms continuous solid solutions with the isostructural compounds CoTi and NiTi between 800 and 900 °C [23,24]. This phase is referred to as FeTi rather than (Fe+Ni+Co+Cu)Ti in the text and figures for simplicity.

The other two phases next to the Fe_2Ti layer are in the form of particles with a diameter up to ~350 nm, being either in contact with the Fe_2Ti layer or separated from this layer by very small distances. The majority of these particles are Ni-rich, with a typical composition of 48Ni–25Ti–11Cu–9Co–7Fe at.%. The crystal structure of this phase has been identified as that of Ni_3Ti (hexagonal, $P6_3/mmc$, space group 194) with the lattice parameters a = 5.2 Å and c = 8.4 Å; a selection of indexed electron diffraction patterns from this phase is shown in Figure 6. Although a significant amount of Ni in Ni_3Ti is substituted by other transition metals such as Cu, Co and Fe, this phase is referred to as Ni_3Ti for simplicity. A very small proportion of the particles next to the Fe_2Ti layer in joints which were brazed at 815 °C for a nominal 1 s and indeed at temperatures up to 845 °C for up to 15 min have a composition of 33Cu–31Ni–32Ti–2Co–1Fe–1Al at.%. These particles were identified as the equiatomic CuNiTi phase (tetragonal, $I4/mmm$, space group 139) with the lattice parameters a = 3.1 Å and c = 8.0 Å; a selection of electron indexed diffraction patterns from this phase

is shown in Figure 7.

There are two significant differences in the interfacial structures of the joint after increasing τ to 1 min at a T_p of 815 °C. The first difference is mainly a result of lateral growth of the FeTi particles on the Fe_2Ti layer to produce a continuous FeTi layer, which is ~330 nm thick. The second difference is the formation of a 650 nm thick, continuous and polycrystalline layer on the Al_2O_3 to bond the ABA chemically to the Al_2O_3. These microstructural developments at the ABA/Kovar® and ABA/Al_2O_3 interfaces can be seen clearly in the BSEIs shown in Figure 1b.

The crystal structure of the particles on the Al_2O_3 has been identified as that of the diamond-cubic type structure of two M_6X-type compounds in the Ti–Cu–O system, specifically Ti_3Cu_3O and Ti_4Cu_2O (cubic, $Fd\bar{3}m$, space group 227), having a unit cell length that varies between 11.2 and 11.5 Å. A selection of electron diffraction patterns from these particles is shown in Figure 8. The composition of this phase was found to vary considerably across the layer on the Al_2O_3. However, no definitive correlation between its composition and the position at which EDS measurements were taken within the layer could be identified. The EDS measurements consistently indicated that the amount of Ti was approximately equal to the amount of other metals in this phase. For example, the compositions of 42Ti–28Cu–6Ni–5Fe–1Co–5Si–1Al–12O at.% and 44Ti–15Cu–14Ni–10Fe–3Co–2Si–1Al–11O at.% have been measured. These measurements are consistent with the formation of only Ti_3Cu_3O on the Al_2O_3. It is also apparent that some of the Cu in the Ti_3Cu_3O has been substituted for other elements, being mainly Fe and Ni. The presence of Si in this layer is very significant, because it indicates that the glassy secondary phase in the alumina has reacted with the ABA. The amount of Si in this layer varied between ~1 and 5 at.%, with the highest value measured at a region close to SiO_2 in the alumina. Based on these experimental results, it is concluded that the layer on the alumina is a solid solution of several elements such as Si, Al, Fe, Ni and Co in Ti_3Cu_3O, and so it is referred to as Ti_3Cu_3O for simplicity.

A number of isolated particles, some being up to 200 nm in diameter, were found in the Ti_3Cu_3O layer at the grain boundaries, and also close to the Al_2O_3, as shown in Figure 9. The results of an EDS area scan containing one of these particles are also given in Figure 9. The particles contain Ti and O; their chemical composition is

measured as being 67Ti–26O–3Cu–2Fe–1Ni–1Si at.%. Electron diffraction patterns collected from these particles are consistent with a solution of oxygen in α-Ti (hexagonal, $P6_3/mmc$, space group 194), with the lattice parameters a = 2.95 Å and c = 4.85 Å, rather than a Ti–O compound. These particles were not observed in joints that were brazed for 2 min or longer at any T_p used.

A small number of isolated particles were also observed between the Ti_3Cu_3O layer and the Al_2O_3, as shown in Figure 9. EDS analysis indicated that these particles also contained Ti and O. Electron diffraction was used to identify the crystal structure of these particles as that of γ-TiO (cubic, $Fm\bar{3}m$, space group 225, a = 4.3 Å); a selection of electron diffraction patterns is shown in Figure 9. γ-TiO particles were observed on the Al_2O_3 in joints made at a T_p of 815 °C only as a small number of isolated particles, between ~30 nm and ~150 nm wide. The Ag–Cu–Ti/Al_2O_3 interface described here closely resembles the interfacial structures that form in Al_2O_3/Ag–Cu–Ti/Al_2O_3 joints at an early stage of brazing [10].

No further significant changes in the structures of the FeTi, Fe_2Ti and Ti_3Cu_3O layers were identified until τ was increased to 10 min at a T_p of 815 °C. By contrast, some of the Ni_3Ti particles had grown significantly by brazing for 6 min at 815 °C to form rectangular shaped particles, approximately 2 μm × 1 μm in size. After brazing for 10 min at a T_p of 815 °C, a thin broken FeTi layer was typically observed alongside the Fe_2Ti layer, as shown in Figure 1c. A small proportion of the same joint showed no evidence of FeTi on the Fe_2Ti layer. The thicknesses of the FeTi and Fe_2Ti layers as a function of τ for the different T_p used are shown graphically in Figure 10. At a T_p of 815 °C, the thickness of the FeTi layer reduced from ~350 nm until it had disappeared as τ increased from 6 to 15 min. At the same time, the Fe_2Ti layer had grown thicker from ~1.3 to 2.0 μm. A correlation between the growth of Fe_2Ti and the disappearance of FeTi is also found in joints made at a T_p of 845 °C, in which the FeTi layer was observed alongside the Fe_2Ti layer only at a brazing time of 2 min. A single continuous layer of Fe_2Ti was observed on the Kovar® consistently in a joint that was held at 815 °C for 15 min, as shown in Figure 1d. Cracks from the Fe_2Ti/Kovar® interface going through the Fe_2Ti layer to the Fe_2Ti/ABA interface were occasionally observed in this joint (Figure 1d), and also other joints that were brazed for 15 min or longer at a higher

T_p.

The microstructure across the joint became irregular after increasing τ to 30 min at a T_p of 815 °C. Continuous reaction layers of Fe_2Ti and Ti_3Cu_3O were typically seen on the Kovar® and the Al_2O_3, respectively. However, at random positions along the joint the Fe_2Ti layer had separated from the Kovar® carrying Ni_3Ti particles with it into the ABA, as shown in Figure 2a. The result is a complex chain of particles, comprised of Fe_2Ti and Ni_3Ti, in the ABA, which is consistent with reports in the literature [13,14,16–18] of the typical distribution of these phases in a joint. At the same area of the joint, a broken Ti_3Cu_3O layer is observed on the Al_2O_3. Separation of the Fe_2Ti layer from the Kovar® was also occasionally observed in a joint held for 45 min at a T_p of 815 °C. The Fe_2Ti layer typically remained attached to the Kovar® in this joint. At the ABA/Al_2O_3 interface in the same joint, Fe_2Ti particles with the composition 45Fe–31Ti–12Co–11Ni–1Cu at.% were observed between the broken Ti_3Cu_3O layer and the ABA, as shown in Figure 2b. Those Fe_2Ti particles appear to nucleate and grow at the ABA/Al_2O_3 interface, specifically on the Ti_3Cu_3O layer as it breaks down, rather than relocate to the ABA/Al_2O_3 interface from the Fe_2Ti layer on the Kovar®. This has been confirmed by brazing at a higher T_p deliberately to decompose the Ti_3Cu_3O phase completely and produce larger quantities of Fe_2Ti particles at the ABA/Al_2O_3 interface. A detailed account of the decomposition of Ti_3Cu_3O in braze joints is given later in this section, and the process is discussed in section 4.1.2.

3.1.2. Brazing 95 wt.% Al_2O_3 at 845 °C

As expected, increasing T_p to 845 °C resulted in less subtle and more progressive changes in the microstructure of the joint as a function of τ. A collection of BSEIs of cross-sections of 95 wt.% Al_2O_3–Kovar® joints that were held at 845 °C for 2 to 45 min is shown in Figure 11. Continuous reactions layers were observed on both the Kovar® and the Al_2O_3 only in joints that were brazed at T_p for up to 10 min. Brazing for a short time of 2 min at 845 °C formed interfacial structures that were very similar to those formed in a joint using a T_p of 815 °C. A continuous Fe_2Ti layer, ~1.45 μm in thickness, formed on the Kovar®, alongside a 900 nm thick FeTi layer. As τ increased

to 10 min the FeTi layer disappeared to leave a 2.1 μm thick Fe_2Ti layer on the Kovar®. The Ti_3Cu_3O layer on the Al_2O_3 became slightly thicker with this change in τ, increasing from ~650 nm to ~750 nm.

Joints that were brazed for 15 min or longer at a T_p of 845 °C contained overly developed ABA/Kovar® and ABA/Al_2O_3 interfaces. In these joints, the Fe_2Ti layer separated from the Kovar® taking the Ni_3Ti particles with it into the ABA, and/or the Ti_3Cu_3O layer on the Al_2O_3 broke down considerably. The Ti_3Cu_3O phase decomposed completely using a brazing cycle that peaked at 845 °C for 45 min to leave two phases, both being in the form of particles, at the ABA/Al_2O_3 interface, as shown in Figure 11d. Electron diffraction and TEM–EDS have been used to identify Fe_2Ti particles (48Fe–30Ti–10Co–10Ni–2Cu at.%) alongside several nanometre-size γ-TiO particles (50Ti–48O–1Al–1Si at.%) at this overly developed ABA/Al_2O_3 interface.

For a T_p ≤845 °C, the Ti_3Cu_3O layer became thicker as τ increased to 10 min, up to a maximum value of ~1 μm. Unfortunately, our data does not provide definitive results on the kinetics of reaction layer growth at the ABA/Al_2O_3 interface. The thickness of this layer reduces as τ increases further at either T_p. This is because the Ti_3Cu_3O phase is metastable at T_p, i.e. between 815 and 900 °C, and so the Ti_3Cu_3O layer breaks down using long brazing times. The rate of Ti_3Cu_3O decomposition is accelerated by using a higher T_p and the effect of the decomposition process is very noticeable by brazing for ≥30 min at 815 °C, ≥15 min at 845 °C or ≥2 min at between 875 and 900 °C.

3.1.3. Brazing 95 wt.% Al_2O_3 at ≥875 °C

A joint with a completely uniform microstructure has not been produced using a T_p ≥875 °C. Brazing for 2 min at either 875 °C or 900 °C resulted in a joint typically having continuous Fe_2Ti and Ti_3Cu_3O layers on the Kovar® and the Al_2O_3, respectively. There were also areas of this joint having a broken Ti_3Cu_3O layer and a Fe_2Ti layer separated from the Kovar®. Brazing for 15 min or longer at 875 °C produced ABA/Al_2O_3 interfaces having either a broken Ti_3Cu_3O layer with nanometre-size γ-TiO particles between the Ti_3Cu_3O and the Al_2O_3, or Fe_2Ti particles on the Al_2O_3 alongside several smaller γ-TiO particles when the Ti_3Cu_3O phase decomposed

completely.

3.2. Brazing 99.7 wt.% Al_2O_3 to Kovar®

Brazing alumina ceramics containing very low levels of secondary phases to Kovar® was particularly difficult. In all of the joints made using 99.7 wt.% Al_2O_3, there were some sections where the ABA and Al_2O_3 were in contact, but where there was no evidence for the formation of any new phases. Furthermore, no evidence was found of a chemical reaction between 99.7 wt.% Al_2O_3 and the ABA in any joint that was brazed for 2 min at a $T_p \leq 875$ °C or up to 45 min at 815 °C. It would not have been worthwhile to increase T_p to encourage a reaction between the ABA and the Al_2O_3. This is because the Fe_2Ti layer on the Kovar® had already peeled away into the ABA at several positions of a joint that was brazed at 875 °C for 2 min to produce an irregular microstructure. The first sign of a chemical reaction at the ABA/Al_2O_3 interface was found in a joint which was brazed for 15 min at 845 °C. At a section of this joint, a 450 nm thick Ti_3Cu_3O layer, with the composition 45Ti–23Cu–9Ni–5Fe–2Co–2Al–1Si–13O at.%, formed on the Al_2O_3. The Ti_3Cu_3O layer was not continuous across the joint. The microstructure at the ABA/Kovar® interface was also inconsistent across the joint, as a consequence of the Fe_2Ti layer being separated from the Kovar® at random positions. A collection of BSEIs capturing some of the interfacial structures produced in 99.7 wt.% Al_2O_3/Cusil ABA®/Kovar® joints which were brazed at 845 °C for 2 to 45 min is shown in Figure 12. In this composite figure, sections of joints with interfacial phases developed at the ABA/Al_2O_3 interface are shown intentionally.

Increasing τ further had an undesirable effect on the structure of the Ti_3Cu_3O layer on the Al_2O_3. This layer broke down to leave individual Fe_2Ti particles between it and the ABA, along with nanometre-size γ-TiO particles on the alumina.

These brazing experiments indicate that the glassy secondary phase in the 95 wt.% Al_2O_3 helps to bond the ceramic chemically to the ABA at the lowest T_p used. Brazing 95 wt.% Al_2O_3 to Kovar® using Cusil ABA® for short periods of time at temperatures near to the liquidus temperature of the ABA enables a continuous Ti_3Cu_3O layer to form, and be preserved, on the Al_2O_3, and also produces a uniform interfacial structure

at the ABA/Kovar® interface.

4. Discussion

4.1. Formation of the interfacial phases

4.1.1. ABA/Kovar® interface

Melting of the ABA facilitates the diffusion of Ti towards the Kovar® and the Al_2O_3. The rates at which chemical reactions occur at the ABA/Kovar® interface are significantly higher than those at the ABA/Al_2O_3 interface. As a consequence, using a very short τ, <<1 min, only produces chemical bonds between the ABA and Kovar®. A number of binary compounds mainly form on the Kovar® which have one element substituted extensively by several elements from the Kovar® or ABA. Fe_2Ti nucleates first on the Kovar®, presumably by the reaction:

$$2\,Fe + Ti \longrightarrow Fe_2Ti \qquad (1)$$

which has a change in Gibbs free energy (ΔG) of approximately –71 kJ mol^{-1} at 1100 K (based on the Gibbs free energies reported in the work of Barin [28]). At this temperature, which is only slightly higher than the lowest T_p used, a reaction producing FeTi is thermodynamically less favourable, based on having a larger ΔG (approximately –32 kJ mol^{-1}). The Fe_2Ti particles subsequently grow to form a continuous layer on the Kovar®. This layer seems to hinder the diffusion of Ti to the Kovar® significantly, because further growth of this layer normal to the Kovar® appears to cease at a thickness of ~1.3 μm.

In this investigation, the extent to which the composition of the compounds identified at the ABA/Kovar® interface are affected by altering T_p or τ is not clear. This is partly because these compounds form as solid solutions containing considerable and highly variable quantities of elements from the ABA and the Kovar®. This apparently occurs by substitution of one of the elements in the compound by an element that is similar in size. A further complication is that some of these compounds, such as Fe_2Ti

and Ni_3Ti, can evolve in non-stoichiometric forms [21,27]. The homogeneity of Fe_2Ti ranges from ~67 to ~72 at.% Fe at 815 °C, and a number of assessments of the Fe–Ti system suggest this range becomes smaller as temperature decreases [21,22]. In this regard, the particles of α-Ti observed in the Fe_2Ti layer could precipitate out of the Fe_2Ti on cooling the joints from T_p. It is unlikely that these particles are remnants of the active element that has not reacted. This is because similar quantities of α-Ti particles were observed in all of the joints examined by TEM, and also in a 95 wt.% Al_2O_3–Kovar® joint brazed at 845 °C for 100 min.

Various compounds such as FeTi, Ni_3Ti and, to a much lesser extent, CuNiTi subsequently nucleate on the Fe_2Ti layer, possibly by the reactions:

$$Fe + Ti \longrightarrow FeTi \quad (2)$$

$$3\,Ni + Ti \longrightarrow Ni_3Ti \quad (3)$$

$$Cu + Ni + Ti \longrightarrow CuNiTi \quad (4)$$

where ΔG for equation 3 occurring at 1100 K is approximately –115 kJ mol^{-1}. At this temperature, the formation of other Ni–Ti compounds such as NiTi and Ni_2Ti by a reaction between Ni and Ti are less thermodynamically favoured; ΔG values for the formation of Ni_2Ti and NiTi are approximately –69 kJ mol^{-1} and –57 kJ mol^{-1}, respectively. No thermodynamic information could be found on CuNiTi to assess whether reaction 4 is possible at the T_p used. If it is assumed that some extent of local equilibrium exists at the ABA/Kovar® interface so that phase diagrams can be used to explain the development of the interfacial structure, it can be inferred from the Fe–Ni–Ti isothermal sections between 800 and 1000 °C [24] that Fe_2Ti can form on the Kovar®. The Kovar® is considered simply as Fe-rich γ-(Fe,Ni) such as Fe–28 Ni at.%, which is separated from Fe_2Ti by the two-phase region γ + Fe_2Ti. After the formation of Fe_2Ti, the formation of FeTi and Ni_3Ti simultaneously on the Fe_2Ti under equilibrium conditions is possible.

The FeTi particles grow primarily parallel to the Fe_2Ti layer to form another continuous layer. This layer also appears to hinder the diffusion of Ti, now to the

Fe_2Ti/FeTi interface, because the FeTi layer does not continue to grow significantly after becoming continuous. At this point, chemical reactions begin at the ABA/Al_2O_3 interface, which are discussed in section 4.1.2. Elements from the Kovar® continue to diffuse towards the ABA, although now being impeded by the Fe_2Ti and FeTi layers. The Fe_2Ti layer grows significantly thicker, up to ~2 μm, as the FeTi layer disappears. A possible explanation for this is a reaction at the Fe_2Ti/FeTi interface between FeTi and the Fe diffusing from the Kovar®, as described in equation 5.

$$Fe + FeTi \longrightarrow Fe_2Ti \quad (5)$$

This reaction is thermodynamically possible at 1100 K, with a ΔG of approximately −39 kJ mol^{-1}. The thicker Fe_2Ti layer presents a larger diffusion barrier, and so this layer does not continue to grow after the FeTi has reacted. Diffusion of elements such as such as Fe, Ni and Ti through the Fe_2Ti layer appears to cease at this point, because the Ni_3Ti particles on this layer and the Ti_3Cu_3O particles on the Al_2O_3 do not grow further. The evolution of the interfacial phases in a Al_2O_3/Cusil ABA®/Kovar® joint is summarised by the schematic mechanism in Figure 13.

4.1.2. ABA/Al_2O_3 interface

The chemical processes that occur between Cusil ABA® and the Al_2O_3 in Al_2O_3–Kovar® brazed joints are initially very similar to those occurring in Al_2O_3–Al_2O_3 joints made with the same ABA. As a consequence, the microstructures at the ABA/Al_2O_3 interfaces in both joints are very similar at the early stages of brazing. The chemical processes responsible for joining Al_2O_3 to itself have recently been reported [10]. Each process is summarised here together with some subtle differences as a consequence of replacing one Al_2O_3 component by Kovar®.

After the ABA melts, and also sometime after chemical reactions begin at the Kovar® surface, some Ti reacts with the Al_2O_3 component. This reaction occurs primarily with the secondary phases in the Al_2O_3 such as SiO_2. The resultant products are Ti_2O, Si (from SiO_2) and, to a much lesser extent, Al (from Al_2O_3). The majority of

the Si and Al is dissolved into the molten ABA, and presumably the Ti_2O remains in contact with the Al_2O_3. Particles of Ti_2O were identified as a transient phase in this work, only being observed in a 95 wt.% Al_2O_3–Kovar® joint brazed for 1 min at 815 °C (Figure 9). A thin continuous Ti_2O layer probably develops on the Al_2O_3, which subsequently reacts to form a continuous Ti_3Cu_3O layer on the Al_2O_3. This reaction can be described by the schematic equation:

$$Ti_2O + Ti + M' \longrightarrow Ti_3M'_3O \quad (6)$$

where M' is a mixture of several elements, comprised mainly of Cu, but also Ni, Fe, Si and Al. In a number of previous studies [15,16], various quantities of elements from the Kovar®, particularly Ni and Fe, were identified in the reaction layer on the Al_2O_3. This is because Ti_3Cu_3O forms on the Al_2O_3, rather than a titanium oxide, and it can accommodate various elements such as Ni and Fe by a substitution mechanism.

Individual γ-TiO particles were observed between the Ti_3Cu_3O layer and the Al_2O_3 rather than a continuous γ-TiO layer. This is a consequence of Ti reacting with the Kovar® first, and so reducing the quantity of Ti in the ABA, which subsequently reacts at the ABA/Al_2O_3 interface. Two recent assessments of the Al_2O_3/Ag–Cu–Ti/Al_2O_3 configuration provided empirical evidence to suggest γ-TiO forms after the Ti_3Cu_3O layer, by a reaction between Al_2O_3 and Ti diffusing through the Ti_3Cu_3O layer [10,11]. Based on this evidence, a similar reaction might also occur with the secondary phase in the Al_2O_3, and so γ-TiO formation could be represented by the schematic equations:

$$x\,Ti + \tfrac{1}{3}\,Al_2O_3 \longrightarrow Ti_xO + \tfrac{2}{3}\,Al \quad (7)$$

$$x\,Ti + \tfrac{1}{2}\,SiO_2 \longrightarrow Ti_xO + \tfrac{1}{2}\,Si \quad (8)$$

where $x \approx 1$, and the Al and Si can form solid solutions with the titanium oxide or Ti_3Cu_3O. Estimations of ΔG for equations 7 and 8 occurring at 1100 K are approximately 6 kJ mol^{-1} and –82 kJ mol^{-1}, respectively, on the basis of oxidation-reduction reactions alone using crystalline oxides to produce the stoichiometric

compound TiO. These estimations suggest the formation of γ-TiO in this work might occur by equation 8 rather than 7. However, such a simple assessment of these equations does not take into account the free energies of solution of Al or Si in the oxides at the ABA/Al_2O_3 interface or the molten ABA. Since the estimation of ΔG for equation 7 is a small positive value, it could therefore be that equation 7 is thermodynamically possible at T_p. No evidence was found of various Si–Ti compounds such as SiTi, Si_2Ti and Si_3Ti_5 at the ABA/Al_2O_3 interface. These Si–Ti compounds are thermodynamically less likely to form at around T_p than TiO; the Gibbs free energies of formation at 1100 K for TiO and these Si–Ti compounds are given in Table 3 on a per mole Ti basis for comparison purposes.

One of the main causes of inhomogeneity in the microstructure of a joint is the breakdown of the Ti_3Cu_3O layer on the Al_2O_3. Ti_3Cu_3O is metastable at T_p and eventually breaks down to produce more γ-TiO particles and new Fe_2Ti particles at the ABA/Al_2O_3 interface. The Fe in these Fe_2Ti particles was originally a solute in Ti_3Cu_3O. Increasing the quantity of Ti in the ABA as an approach to lengthen the time taken before significant decomposition of the Ti_3Cu_3O layer occurs is discussed in section 4.2. In the same section, conditions for T_p and τ to produce Al_2O_3/Cusil ABA®/Kovar® joints with well-developed uniform microstructures are given.

4.2. Morphological features of the interfacial phases and joint strength

It was expected that the thickness of the Ti_3Cu_3O layer would be limited as a consequence of the chemical reactions between the Kovar® and ABA consuming some of the Ti. The maximum thickness of this layer was ~850 nm. This is considerably lower than the maximum thickness of the Ti_3Cu_3O layers formed in a Al_2O_3–Al_2O_3 joint made using the same ABA and ceramic used in this work, which was ~1.5 μm after brazing for 2 min at 875 °C [11]. This difference in thickness is significant because the Ti_3Cu_3O phase is not stable at T_p and as a consequence it breaks down to form other phases at the ABA/Al_2O_3 interface. The temperature at which the chemical decomposition of Ti_3Cu_3O begins should not be affected by its thickness, but a thinner Ti_3Cu_3O layer would break down faster. This could adversely affect the performance of a joint, particularly if it must be airtight. In the 95 wt.% Al_2O_3–Kovar® joint, the

Ti_3Cu_3O layer broke down completely so that there was no evidence of it at the ABA/Al_2O_3 interface after ~45 min at 845 °C. Only partial decomposition of the Ti_3Cu_3O layers in a Al_2O_3–Al_2O_3 joint made using the same ABA and ceramic occurred after brazing between 845 and 875 °C for the same length of time [11].

It has been shown that continuous Ti_3Cu_3O layers prevail in Al_2O_3/Ag–Cu–Ti/Al_2O_3 joints for longer periods of time at the liquidus temperature of the Ag–Cu–Ti-based ABA by essentially increasing the quantity of the active element [11]. This was achieved by changing the ABA from Cusil ABA® to Ticusil®. As a consequence, thicker Ti_3Cu_3O layers formed, and this ultimately lengthened the time taken to break the Ti_3Cu_3O down into a noticeably broken layer by several minutes. Such a modification to the Al_2O_3/Ag–Cu–Ti/Kovar® joint could help to produce a thicker Ti_3Cu_3O layer, and so preserve it as a continuous layer for longer periods of time at T_p. However, this would also have the undesirable effect of increasing the quantity of the brittle phases formed at the ABA/Kovar® interface.

Another cause of inhomogeneity in the microstructure of a joint is the separation of the Fe_2Ti layer from the Kovar®, which typically coincides with the breakdown of the Ti_3Cu_3O layer on the Al_2O_3. This occurs after the Fe_2Ti layer develops fully into a 2 μm thick layer, together with the development of cracks in this layer. Very little evidence of deformation of Fe_2Ti was observed by TEM, suggesting this phase does not help to any significant extent to dissipate any residual stresses in the joint. Breakdown of the Ti_3Cu_3O layer on the Al_2O_3, together with fracture and separation of the Fe_2Ti layer, can be avoided by brazing joints at temperatures close to the liquidus temperature of the ABA for short periods of time. For this particular joint, this can be achieved using a T_p between 820 and 830 °C and τ between 2 and 8 min. These conditions should also produce uniform microstructures at both interfaces. In practice, the size of the joint will also influence the precise brazing conditions used. This is because any temperature gradients across the joint should be minimised to achieve a uniform microstructure, and this is harder to achieve as the joint becomes larger.

Braze joints of this type will experience tensile stresses in their application, either by an applied load and/or by any residual stresses. Tensile strengths were measured at ambient temperature of 95 wt.% Al_2O_3–Kovar®–95 wt.% Al_2O_3 joints, with Cusil

ABA® positioned between the Kovar® and Al_2O_3. This particular configuration has been used to follow the ASTM F19 standard method for testing the tensile strength of ceramic–metal and ceramic–ceramic brazed bonds [29]. Therefore, the Al_2O_3 components were in the form of ASTM F19 tensile buttons as described in [29] and [11], and so much larger joints were made compared to those used to study the interfacial reaction processes in these joints. As a consequence, significant temperature gradients developed across some of the larger joints. SEM of the joints showed that the interfacial microstructures were far more developed at the edges of these joints, up to ~300 μm into a joint rather than up to ~10 μm for the smaller-sized joints. Three joints were tested for each brazing condition used. These were a T_p of 814 °C with τ equal to 2 or 15 min, a T_p of 828 °C with τ equal to 15 and 45 min, and a T_p of 844 °C with τ equal to 2, 15 and 45 min. The joints held at 844 °C for 2 min had the highest maximum tensile strengths of the order of 60±15 MPa.

5. Conclusions

The interfaces of several Al_2O_3/Cusil ABA®/Kovar® joints have been assessed using a range of electron microscopy-based techniques to determine the identity of the interfacial phases, the chemical processes leading to their evolution and the influence of various brazing parameters, such as T_p and τ, on their structure.

When the ABA melts, the Kovar® first reacts with it to produce quickly a continuous Fe_2Ti layer on the Kovar®. Various compounds subsequently nucleate on this layer such as FeTi and Ni_3Ti. The FeTi develops into a continuous layer on the Fe_2Ti, with larger Ni_3Ti adjacent to it. This layer eventually breaks down to enable the Fe_2Ti layer to grow further. This development coincides with the formation of cracks across the Fe_2Ti layer. Brazing for long periods of time causes the Fe_2Ti layer to separate from the Kovar® and migrate into the ABA, taking the Ni_3Ti particles with it.

The formation and growth of the interfacial phase at the ABA/Kovar® interface consumes a significant proportion of the Ti in the ABA before reactions at the ABA/ Al_2O_3 interface begin. As a consequence, a thinner reaction layer develops on the Al_2O_3. This layer has been identified as a solid solution of elements from the Kovar® such as Fe and Ni in Ti_3Cu_3O. The formation of Ti_3Cu_3O is facilitated greatly by the

glassy secondary phases in the Al_2O_3 such as SiO_2. To a lesser extent, individual γ-TiO nanoparticles were identified on the Al_2O_3. Therefore, the addition of Kovar® next to the ABA does not change the intrinsic chemical reactions occurring at the ABA/Al_2O_3 interface. However, the extent to which the Ti_3Cu_3O layer grows is limited by the presence of the Kovar®. Since Ti_3Cu_3O is metastable at T_p, it consequently breaks down faster, producing more γ-TiO and new Fe_2Ti particles at the ABA/Al_2O_3 interface. Brazing with an ABA containing larger amounts of Ti should produce a thicker Ti_3Cu_3O layer and this might help to prolong its breakdown into a noticeably broken layer.

Brazing of Al_2O_3 to Kovar® with Cusil ABA® has been performed successfully in terms of microstructural development using a ceramic component containing ~5 wt.% secondary phase such as SiO_2. The secondary phase helps to bond the ceramic chemically to the ABA. Joints with uniform microstructures containing continuous reaction layers at both interfaces were only produced by brazing for short periods of time using a T_p close to the liquidus temperature of the ABA. For this particular joint, the formation of overly developed interfaces with a broken Ti_3Cu_3O layer, or fracture of the Fe_2Ti layer and separation of this layer from the Kovar® can be avoided by using a T_p between 820 and 830 °C and τ between 2 and 8 min.

Acknowledgements

We are grateful for the contribution and support for this study by AWE plc.

References

[1] E. Dörre and H. Hübner, *Alumina: Processing, Properties, and Applications*, Springer, Berlin and Heidelberg, 2011.

[2] J.A. Fernie, R.A.L. Drew, and K.M. Knowles, *Joining of engineering ceramics*, Int. Mater. Rev. 54 (2009), pp. 283–331.

[3] K. Suganuma, T. Okamoto, M. Koizumi, and M. Shimada, *Effect of thickness on direct bonding of silicon nitride to steel*, J. Am. Ceram. Soc. 68 (1985), pp. C-334–C-335.

[4] J.A. Fernie and W.B. Hanson, *Best practice for producing ceramic-metal bonds*,

Ind. Ceram. 19 (1999), pp. 172–175.
[5] R.W. Johnson, *Electronic packaging approaches for high-temperature environments*, in *Extreme Environment Electronics*, J.D. Cressler and H.A. Mantooth, eds., CRC Press - Taylor & Francis Group, Boca Raton, 2012, pp. 777–790.
[6] J.D. Cawley, *Binary oxide ceramics: Al_2O_3, ZrO_2, structure and properties of*, in *Concise Encyclopedia of the Structure of Materials*, J.W. Martin, ed., Elsevier, Amsterdam, 2007, pp. 21–30.
[7] J. Stephens, S. Burchett, and W. Jones, *Stress relaxation of braze joints*, The First Joint ASME/JSME Conference on Electronic Packaging, Milpitas, CA, 1992.
[8] H.J. Nolte, Metalized ceramic, US Patent 2667432, 1954.
[9] A.W. Hey, *Metallizing ceramic surfaces*, in *Joining of Ceramics*, M.G. Nicholas, ed., Chapman & Hall, London, 1990, pp. 56–72.
[10] M. Ali, K.M. Knowles, P.M. Mallinson, and J.A. Fernie, *Interfacial reactions between sapphire and Ag–Cu–Ti-based active braze alloys*, Acta Mater. 103 (2016), pp. 859–869.
[11] M. Ali, K.M. Knowles, P.M. Mallinson, and J.A. Fernie, *Microstructural evolution and characterisation of interfacial phases in Al_2O_3/Ag–Cu–Ti/ Al_2O_3 braze joints*, Acta Mater. 96 (2015), pp. 143–158.
[12] J.J. Stephens, P.T. Vianco, P.F. Hlava, and C.A. Walker, *Microstructure and performance of Kovar/alumina joints made with silver-copper base active metal braze alloys*, International Brazing and Soldering Conference, Albuquerque, NM, 2000.
[13] P.T. Vianco, J.J. Stephens, P.F. Hlava, and C.A. Walker, *A barrier layer approach to limit Ti scavenging in FeNiCo/Ag-Cu-Ti/Al_2O_3 active braze joints*, Weld. J. 82 (2003), pp. 252S–262S.
[14] P.T. Vianco, J.J. Stephens, P.F. Hlava, and C.A. Walker, *Titanium scavenging in Ag-Cu-Ti active braze joints*, Weld. J. 82 (2003), pp. 268S–277S.
[15] J. Schilm, A. Goldberg, U. Partsch, W. Dürfeld, D. Arndt, A. Pönicke, and A. Michaelis, *Joining technologies for a temperature-stable integration of a LTCC-based pressure sensor*, J. Sens. Sens. Syst. 5 (2016), pp. 73–83.
[16] Y. Wang, J.C. Feng, L.X. Zhang, P. He, and J.H. Zhang, *Microstructure of alumina ceramic/Ag–Cu–Ti brazing alloy/Kovar alloy joint*, Mater. Sci. Technol. 23 (2007), pp. 320–323.
[17] H. Klose, H. Podlesak, and B. Wielage, *Reaction layer formation on the metal*

side of active brazed metal-ceramic joints, Joining, Ceramics, Glass and Metal: 5th International Conference, Jena, Thuringia, 1997.

[18] R.M. Do Nascimento, A.E. Martinelli, A.J. De A. Buschinelli, and A.N. Klein, *Brazing Al_2O_3 to sintered Fe-Ni-Co alloys*, J. Mater. Sci. 34 (1999), pp. 5839–5845.

[19] J.J. Stephens, F.M. Hosking, C.A. Walker, E.C. Dudley, and F.G. Yost, *The evolution of a ternary Ag-Cu-Zr active braze filler metal for Kovar™/alumina braze joints*, 3rd International Brazing and Soldering Conference, San Antonio, TX, 2006.

[20] D. Tomus and H.P. Ng, *In situ lift-out dedicated techniques using FIB–SEM system for TEM specimen preparation*, Micron 44 (2013), pp. 115–119.

[21] H. Bo, J. Wang, L. Duarte, C. Leinenbach, L.B. Liu, H.S. Liu, and Z.P. Jin, *Thermodynamic re-assessment of Fe–Ti binary system*, Trans. Nonferrous Met. Soc China 22 (2012), pp. 2204–2211.

[22] L.F.S. Dumitrescu and M. Hillert, *Comparison of Fe-Ti assessments*, J. Phase Equilibria 5 (1998), pp. 441–448.

[23] V. Raghavan, *Co-Fe-Ti (cobalt-iron-titanium)*, J. Phase Equilibria 24 (2003), pp. 175–176.

[24] L.I. Duarte, U.E. Klotz, C. Leinenbach, M. Palm, F. Stein, and J.F. Löffler, *Experimental study of the Fe–Ni–Ti system*, Intermet. 18 (2010), pp. 374–384.

[25] V. Raghavan, *Cu-Fe-Ti (copper-iron-titanium)*, J. Phase Equilibria 23 (2002), pp. 172–174.

[26] J.L. Murray, *The Co-Ti (cobalt-titanium) system*, Bull. Alloy Phase Diagrams 3 (1982), pp. 74–85.

[27] H. Okamoto, *Supplemental literature review of binary phase diagrams: Au-Ce, B-Pr, Bi-Gd, Bi-Ho, Cd-Sr, Ga-Ti, Gd-Pb, Gd-Ti, Mg-Mn, Mn-Nd, Nd-Ni, and Ni-Ti*, J. Phase Equilibria Diffus. 36 (2015), pp. 390–401.

[28] I. Barin, *Thermodynamic Data of Pure Substances*, 3rd ed., VCH Verlagsgesellschaft mbH, Weinheim, 1995.

[29] *ASTM F19-64 (2005)e1, Standard Test Method for Tension and Vacuum Testing Metallized Ceramic Seals*, ASTM International, Pennsylvania, USA, 2005; available at http://www.astm.org

Figure Captions

Figure 1. BSEIs of cross-sections of 95 wt.% Al_2O_3/Cusil ABA®/Kovar® joints that were held at 815 °C for a) 0 min, b) 1 min, c) 10 min and d) 15 min.

Figure 2. BSEIs of cross-sections of 95 wt.% Al_2O_3/Cusil ABA®/Kovar® joints that were held at 815 °C for a) 30 min and b) 45 min.

Figure 3. a) TEM bright field image capturing a region of Cusil ABA®/Kovar® interface in a joint which was held at 815 °C for 15 min, along with electron diffraction patterns from Fe_2Ti with the zone axes b) $[2\bar{1}\bar{1}0]$, c) $[5\bar{4}\bar{1}0]$ and d) $[1\bar{1}00]$; 000*l* reflections, where $l \neq 2n$, appear in 3b) and 3c) by double diffraction.

Figure 4. a) Annular dark-field image capturing a small area of the ABA/Kovar® interface formed in a 95 wt.% Al_2O_3/Cusil ABA®/Kovar® joint that was brazed for 2 min at 845 °C, along with b–g) EDS maps showing the distribution of several elements in the interfacial phases; stacking faults in the Fe_2Ti particles appear as striations. Electron diffraction patterns from α-Ti particles, located inside the Fe_2Ti layer, with the zone axes h) $[\bar{1}2\bar{1}3]$ and i) $[\bar{2}4\bar{2}3]$ are shown schematically to identify the relevant reflections clearly.

Figure 5. Electron diffraction patterns from FeTi with the zone axes a) $[11\bar{1}]$, b) $[31\bar{1}]$ and c) [100].

Figure 6. a) TEM bright field image of a Ni_3Ti particle in a joint which was held at 815 °C for 15 min, along with electron diffraction patterns with the zone axes b) $[2\bar{1}\bar{1}0]$ and c) $[4\bar{2}\bar{2}3]$. A schematic diagram of 6b) is given to indicate the positions of reflections appearing with very low intensity. Streaking in 6b) is a consequence of faulting on the {0001} planes.

Figure 7. Electron diffraction patterns from a CuNiTi particle found next to the Fe_2Ti layer in a 95 wt.% Al_2O_3/Cusil ABA®/Kovar® joint, which was brazed for 2 min at 845 °C, with the zone axes a) [031], b) [331] and c) [111].

Figure 8. Electron diffraction patterns from Ti_3Cu_3O with the zone axes a) [311], b) [100] and c) [110].

Figure 9. a) Annular dark-field image capturing a small area of the ABA/Al_2O_3 interface formed in a 95 wt.% Al_2O_3/Cusil ABA®/Kovar® joint that was brazed for 1

min at 815 °C, along with b–g) EDS maps of a α-Ti particle located in the Ti_3Cu_3O reaction layer. Electron diffraction patterns from a γ-TiO particle, located between the Ti_3Cu_3O layer and the Al_2O_3, with the zone axes h) [100] and i) [110] are given.

Figure 10. Thicknesses of the a) FeTi and b) Fe_2Ti layers formed in 95 wt.% Al_2O_3/Cusil ABA®/Kovar® joints which were brazed at a T_p between 815 and 900 °C for 0 to 45 min.

Figure 11. BSEIs of cross-sections of 95 wt.% Al_2O_3/Cusil ABA®/Kovar® joints that were held at 845 °C for a) 2 min, b) 10 min, c) 15 min and d) 45 min.

Figure 12. BSEIs of cross-sections of 99.7 wt.% Al_2O_3/Cusil ABA®/Kovar® joints which were held at 845 °C for a) 2 min, b) 15 min, c) 30 min and d) 45 min, capturing specifically areas of joints having developed interfacial phases at the ABA/Al_2O_3 interface.

Figure 13. Schematic mechanism for the evolution of the interfacial phases in a 95 wt.% Al_2O_3/Cusil ABA®/Kovar® joint; the Al_2O_3 contains silicon and calcium oxides as secondary phases. Dashed arrows are used to indicate the diffusion of chemical elements and solid arrows are used to label phases. Further details are explained in section 4.1.

Table 1. Chemical composition of the 95 wt.% and 99.7 wt.% Al_2O_3 components used in wt.%. Average values from 30 electron microprobe measurements with errors of ± one standard deviation are reported. *The quantities of these elements were below or approximately equal to the detection limit.

Al_2O_3 purity/ wt.% Al_2O_3	**Al**	**O**	**Si**	**Na**	**Mg**	**Ca**	**Fe**
99.7	55.4 ±1.3	44.0 ±1.5	0.2 ±0.1	0.0*	0.3 ±0.1	0.0*	0.0*
95	52.3 ±1.5	43.2 ±1.9	1.9 ±0.3	0.1 ±0.06	0.4 ±0.2	1.9 ±0.2	0.2 ±0.1

Table 2. T_p and τ used to braze 95 and 99.7 wt.% Al_2O_3.

	815 °C	**845 °C**	**875 °C**	**900 °C**
0 min	95 wt.%	–	–	–
1 min	95 wt.%	–	–	–
2 min	95 and 99.7 wt.%	95 and 99.7 wt.%	95 and 99.7 wt.%	95 wt.%
6 min	95 wt.%	–	–	–
10 min	95 and 99.7 wt.%	95 and 99.7 wt.%	–	–
15 min	95 and 99.7 wt.%	95 and 99.7 wt.%	95 and 99.7 wt.%	–
30 min	95 and 99.7 wt.%	95 and 99.7 wt.%	95 wt.%	–
45 min	95 and 99.7 wt.%	95 and 99.7 wt.%	95 wt.%	–

Table 3. Gibbs free energies of formation at 1100 K for TiO and various Si–Ti compounds [28] (data for $SiTi_3$ and Si_4Ti_5 is unavailable).

Reaction	**ΔG/ kJ mol^{-1} Ti**
$Ti + \frac{1}{2} O_2 \longrightarrow TiO$	–437
$Si + Ti \longrightarrow SiTi$	–129
$2\ Si + Ti \longrightarrow Si_2Ti$	–127
$\frac{3}{5} Si + Ti \longrightarrow \frac{1}{5} Si_3Ti_5$	–118

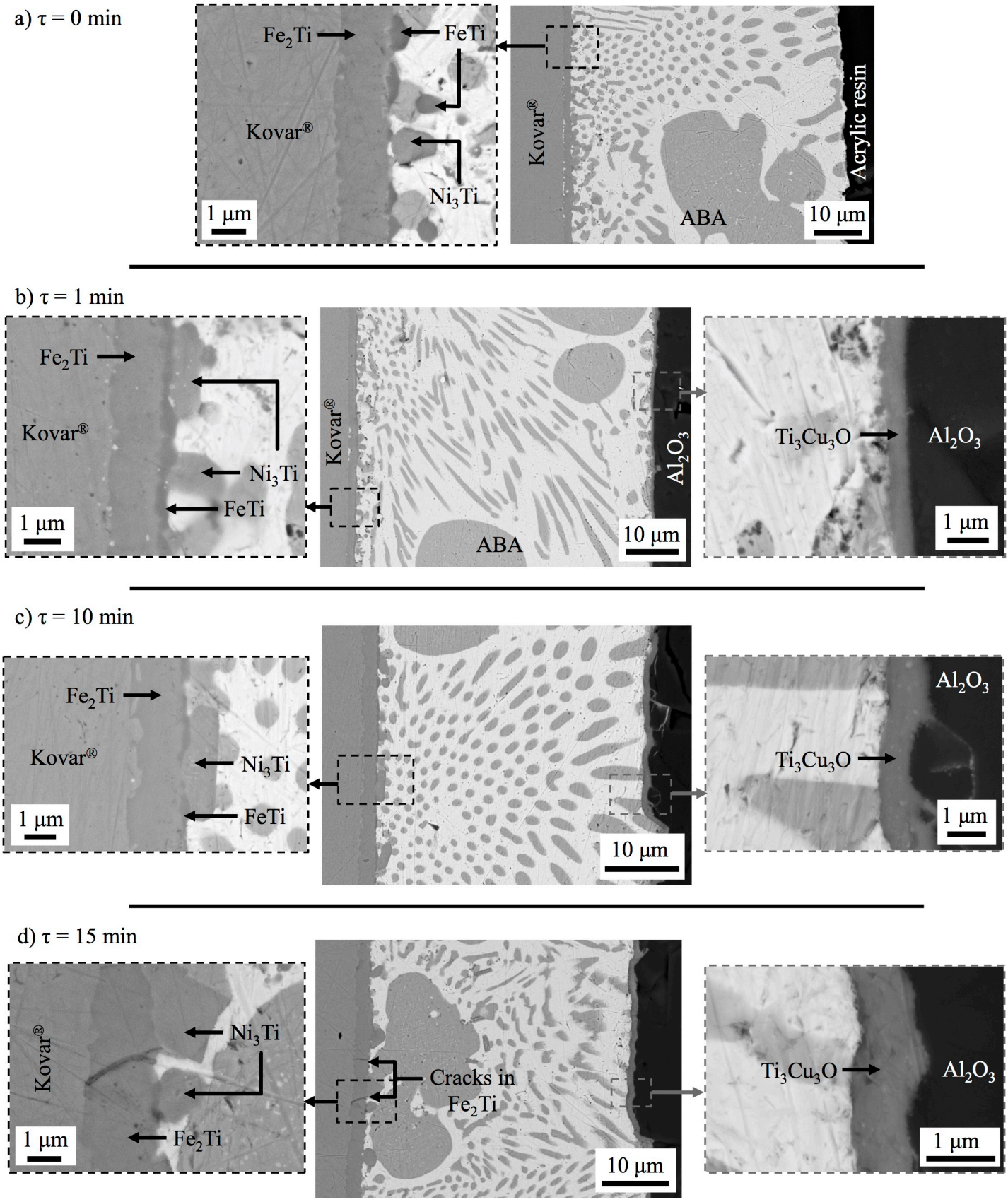

Figure 1. BSEIs of cross-sections of 95 wt.% Al_2O_3/Cusil ABA®/Kovar® joints that were held at 815 °C for a) 0 min, b) 1 min, c) 10 min and d) 15 min.

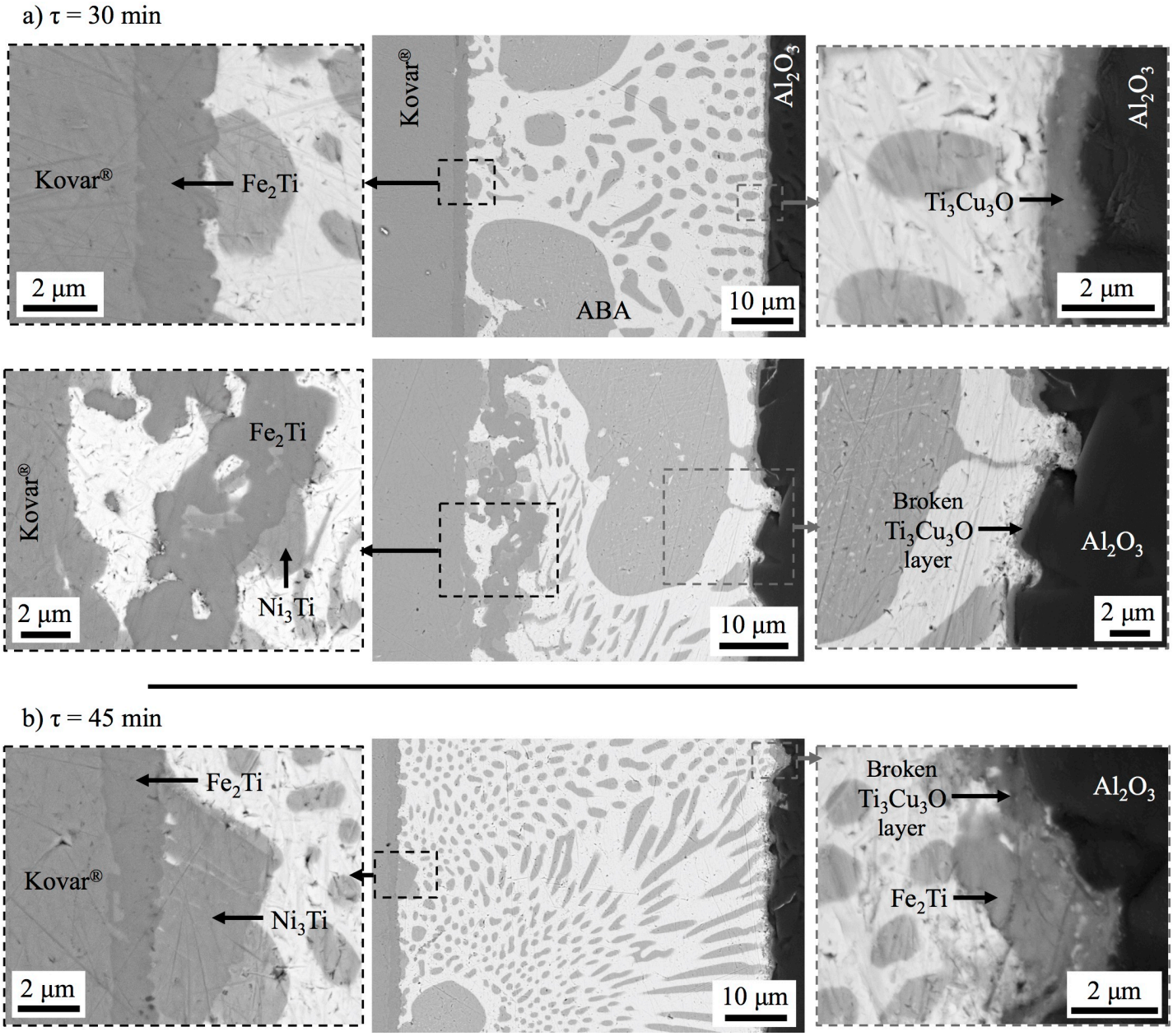

Figure 2. BSEIs of cross-sections of 95 wt.% Al_2O_3/Cusil ABA®/Kovar® joints that were held at 815 °C for a) 30 min and b) 45 min.

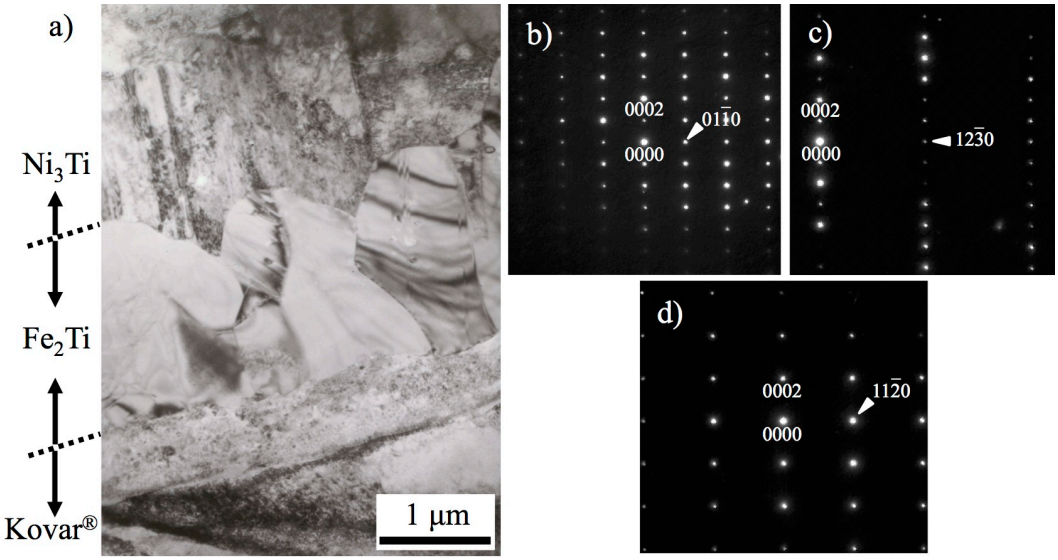

Figure 3. a) TEM bright field image capturing a region of Cusil ABA®/Kovar® interface in a joint which was held at 815 °C for 15 min, along with electron diffraction patterns from Fe_2Ti with the zone axes b) $[2\bar{1}\bar{1}0]$, c) $[5\bar{4}\bar{1}0]$ and d) $[1\bar{1}00]$; $000l$ reflections, where $l \neq 2n$, appear in 3b) and 3c) by double diffraction.

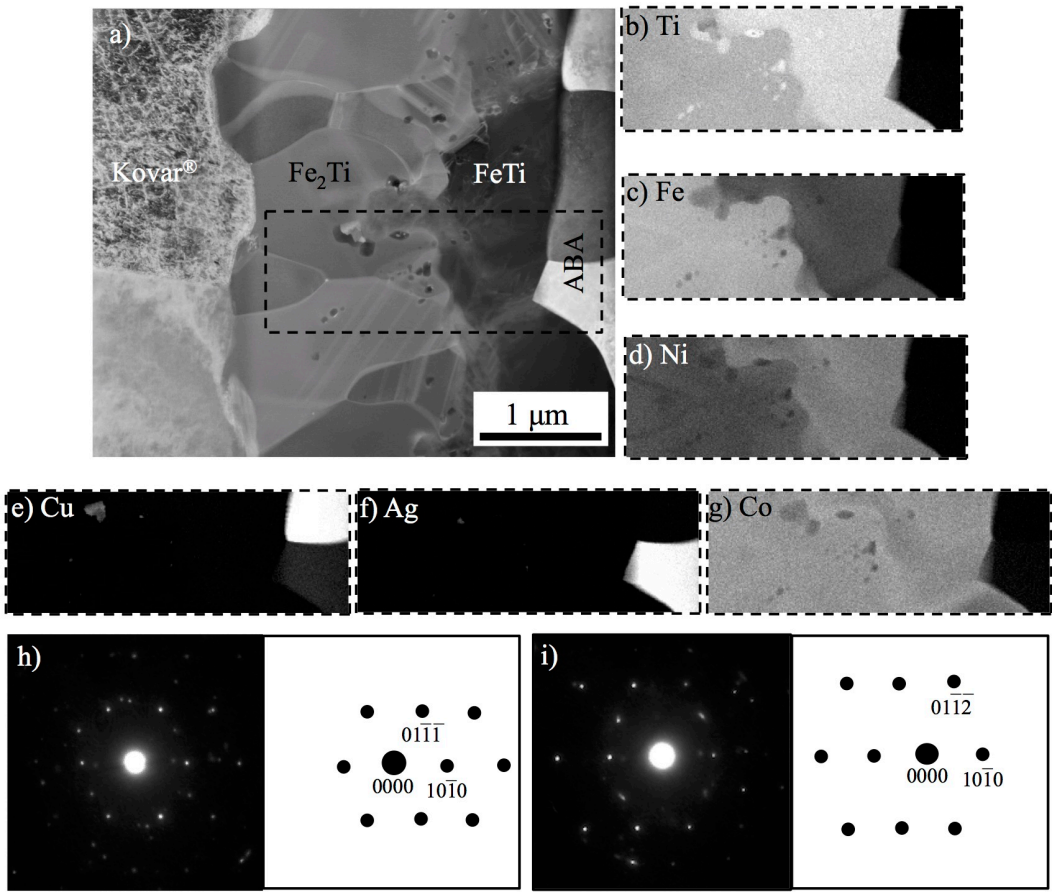

Figure 4. a) Annular dark-field image capturing a small area of the ABA/Kovar® interface formed in a 95 wt.% Al_2O_3/Cusil ABA®/Kovar® joint that was brazed for 2 min at 845 °C, along with b–g) EDS maps showing the distribution of several elements in the interfacial phases; stacking faults in the Fe_2Ti particles appear as striations. Electron diffraction patterns from α-Ti particles, located inside the Fe_2Ti layer, with the zone axes h) $[\bar{1}2\bar{1}3]$ and i) $[\bar{2}4\bar{2}3]$ are shown schematically to identify the relevant reflections clearly.

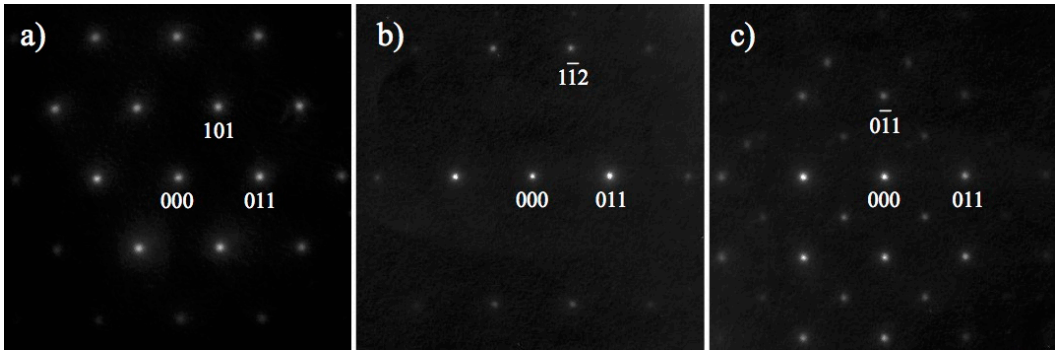

Figure 5. Electron diffraction patterns from FeTi with the zone axes a) [11$\bar{1}$], b) [31$\bar{1}$] and c) [100].

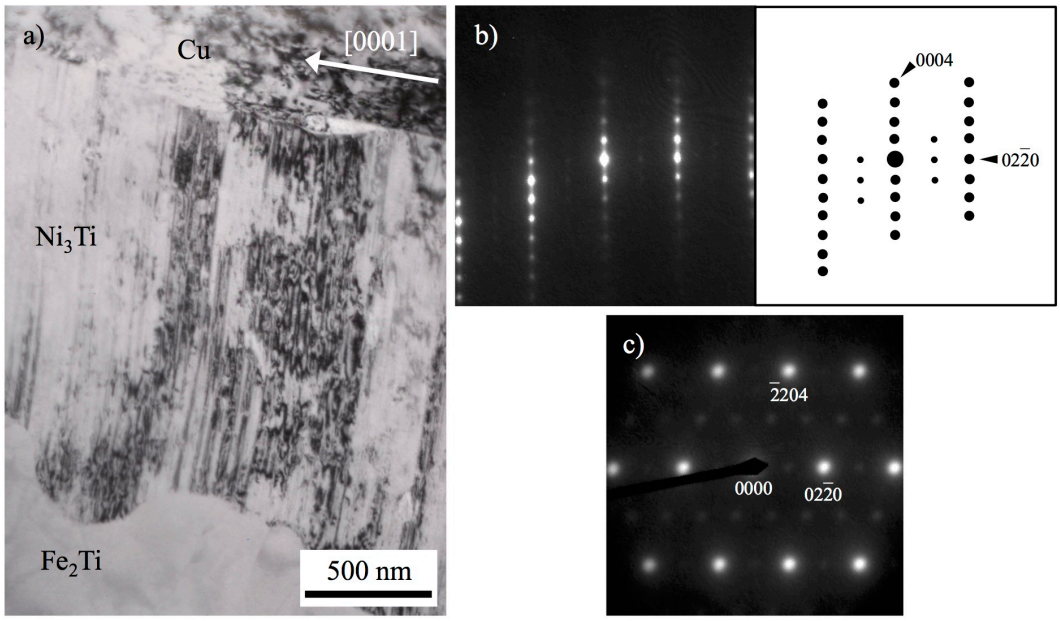

Figure 6. a) TEM bright field image of a Ni_3Ti particle in a joint which was held at 815 °C for 15 min, along with electron diffraction patterns with the zone axes b) $[2\bar{1}\bar{1}0]$ and c) $[4\bar{2}\bar{2}3]$. A schematic diagram of 6b) is given to indicate the positions of reflections appearing with very low intensity. Streaking in 6b) is a consequence of faulting on the {0001} planes.

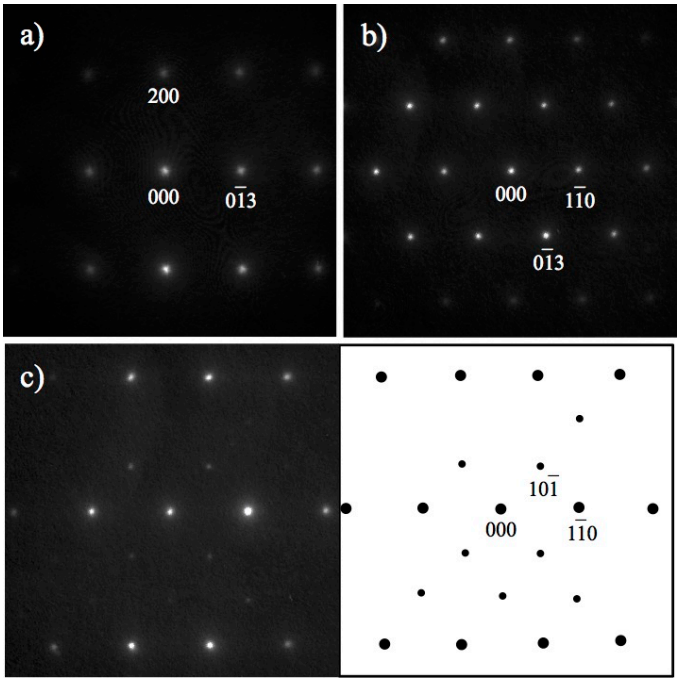

Figure 7. Electron diffraction patterns from a CuNiTi particle found next to the Fe_2Ti layer in a 95 wt.% Al_2O_3/Cusil ABA®/Kovar® joint, which was brazed for 2 min at 845 °C, with the zone axes a) [031], b) [331] and c) [111].

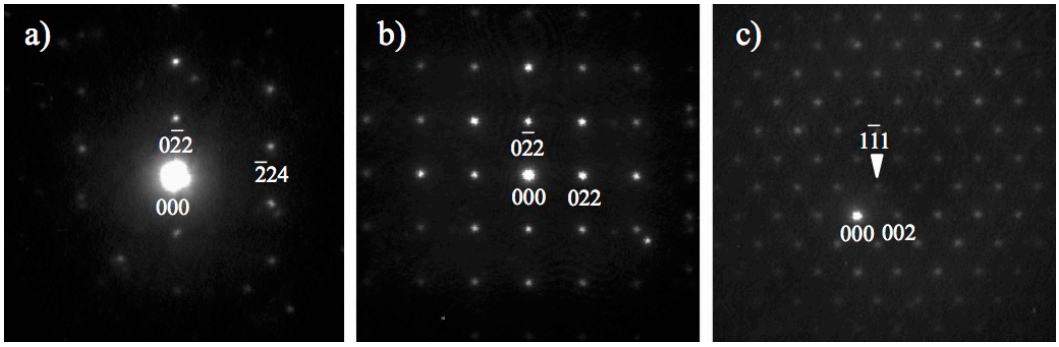

Figure 8. Electron diffraction patterns from Ti_3Cu_3O with the zone axes a) [311], b) [100] and c) [110].

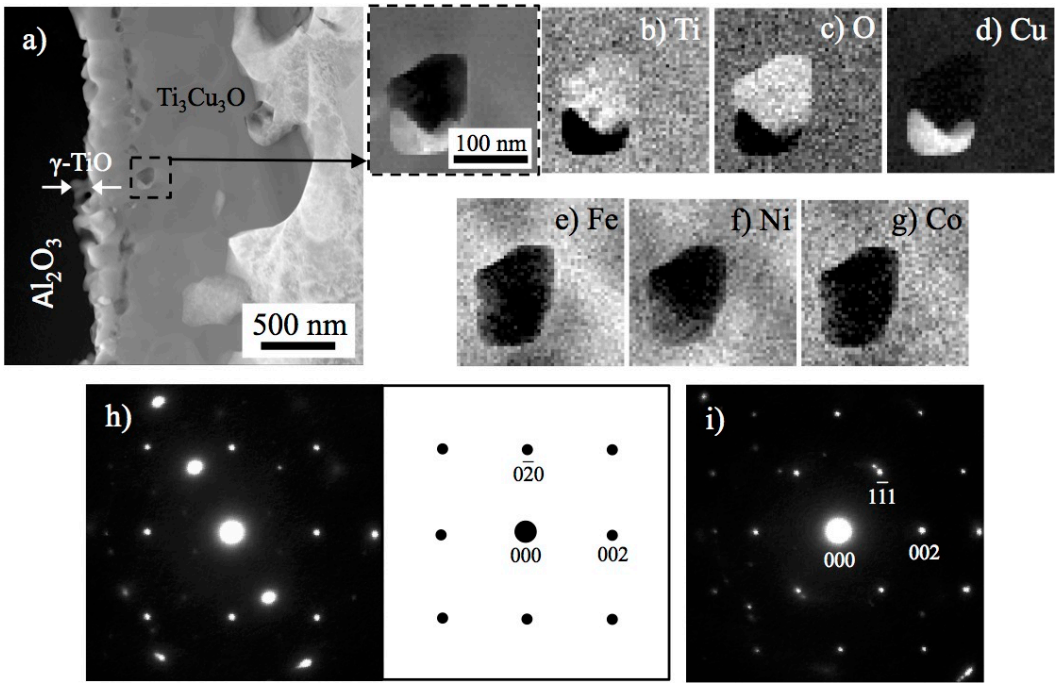

Figure 9. a) Annular dark-field image capturing a small area of the ABA/Al_2O_3 interface formed in a 95 wt.% Al_2O_3/Cusil ABA®/Kovar® joint that was brazed for 1 min at 815 °C, along with b–g) EDS maps of a α-Ti particle located in the Ti_3Cu_3O reaction layer. Electron diffraction patterns from a γ-TiO particle, located between the Ti_3Cu_3O layer and the Al_2O_3, with the zone axes h) [100] and i) [110] are given.

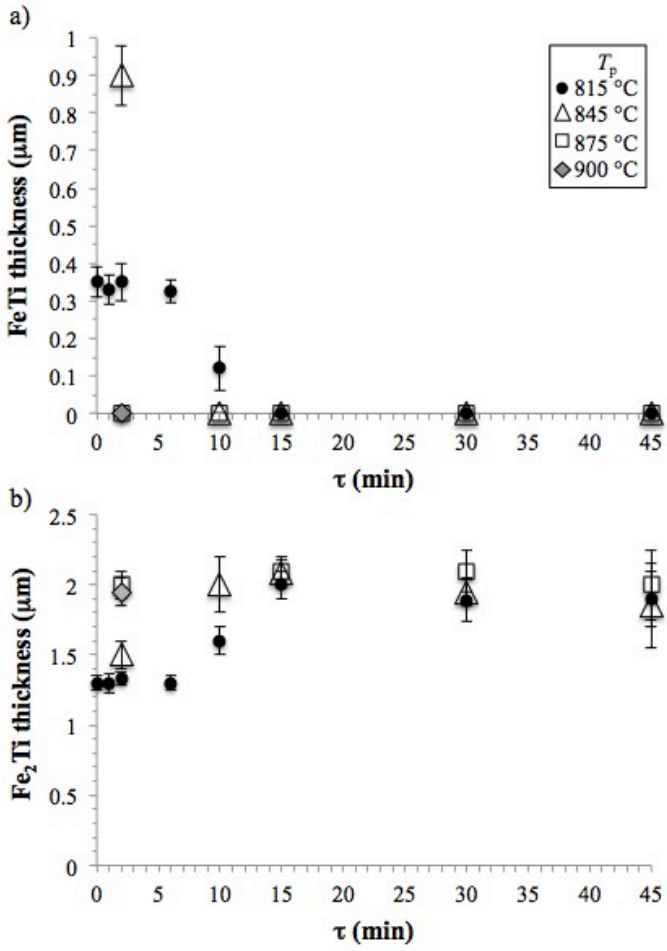

Figure 10. Thicknesses of the a) FeTi and b) Fe_2Ti layers formed in 95 wt.% Al_2O_3/Cusil ABA®/Kovar® joints which were brazed at a T_p between 815 and 900 °C for 0 to 45 min.

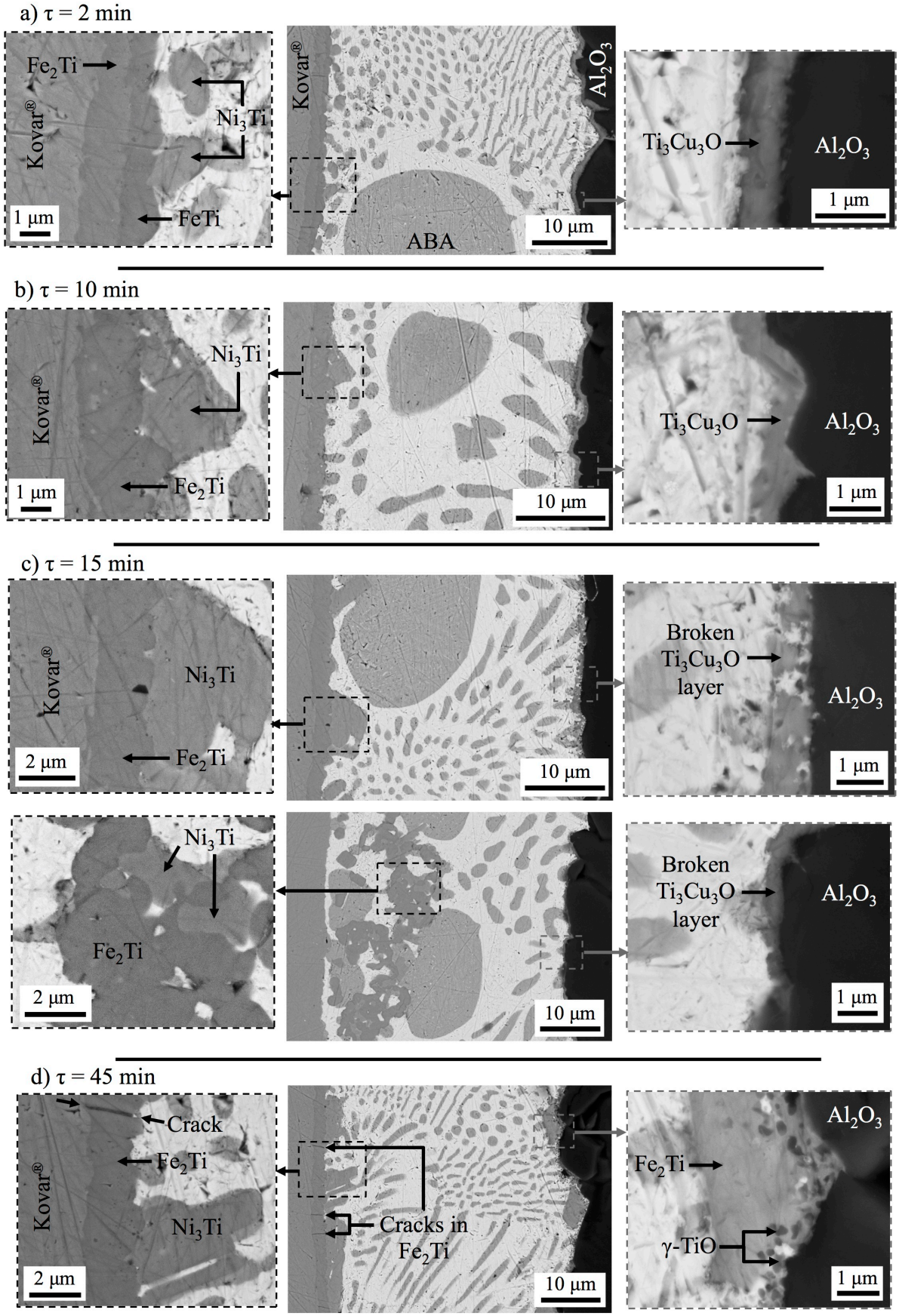

Figure 11. BSEIs of cross-sections of 95 wt.% Al_2O_3/Cusil ABA®/Kovar® joints that were held at 845 °C for a) 2 min, b) 10 min, c) 15 min and d) 45 min.

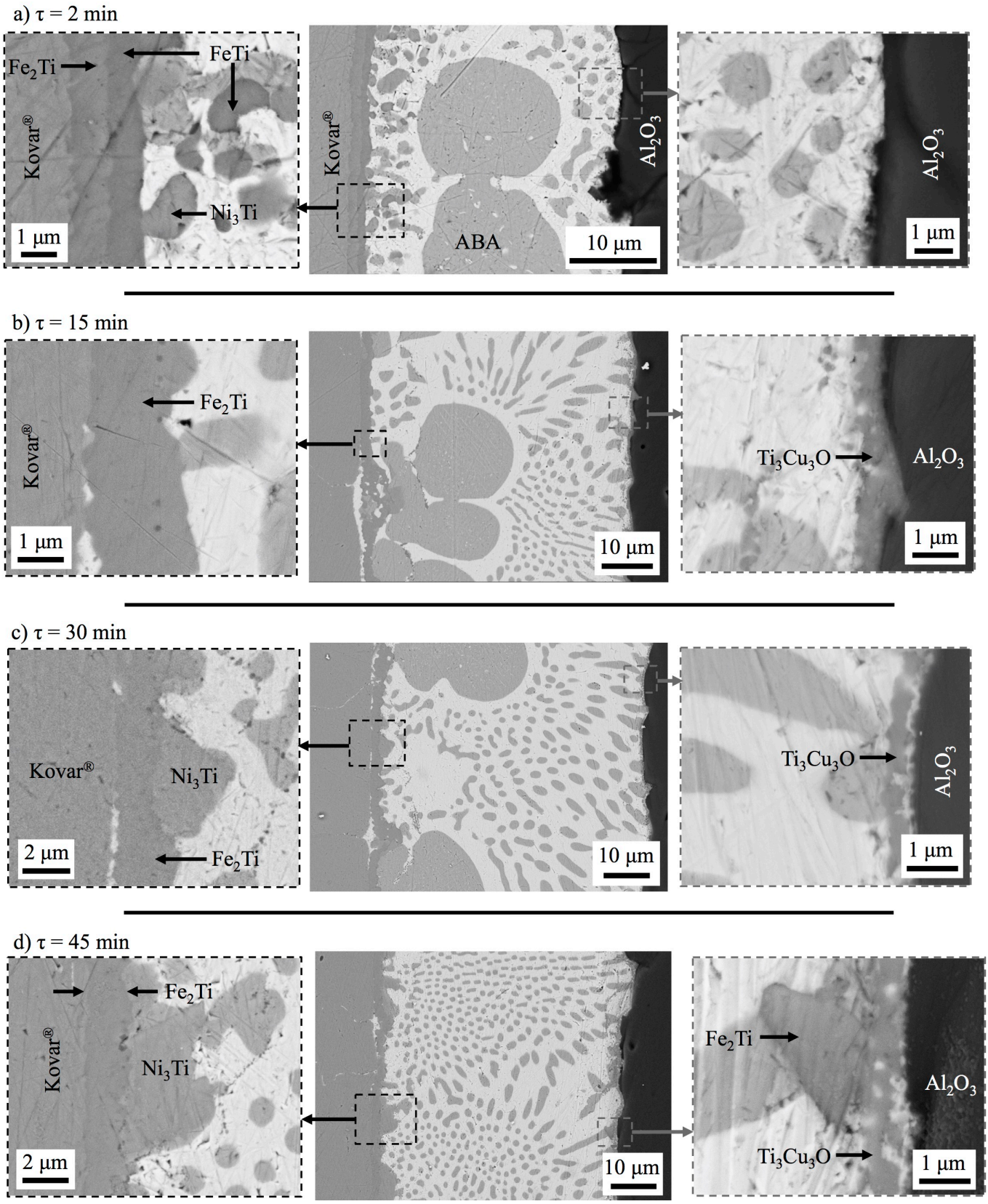

Figure 12. BSEIs of cross-sections of 99.7 wt.% Al_2O_3/Cusil ABA®/Kovar® joints which were held at 845 °C for a) 2 min, b) 15 min, c) 30 min and d) 45 min, capturing specifically areas of joints having developed interfacial phases at the ABA/Al_2O_3 interface.

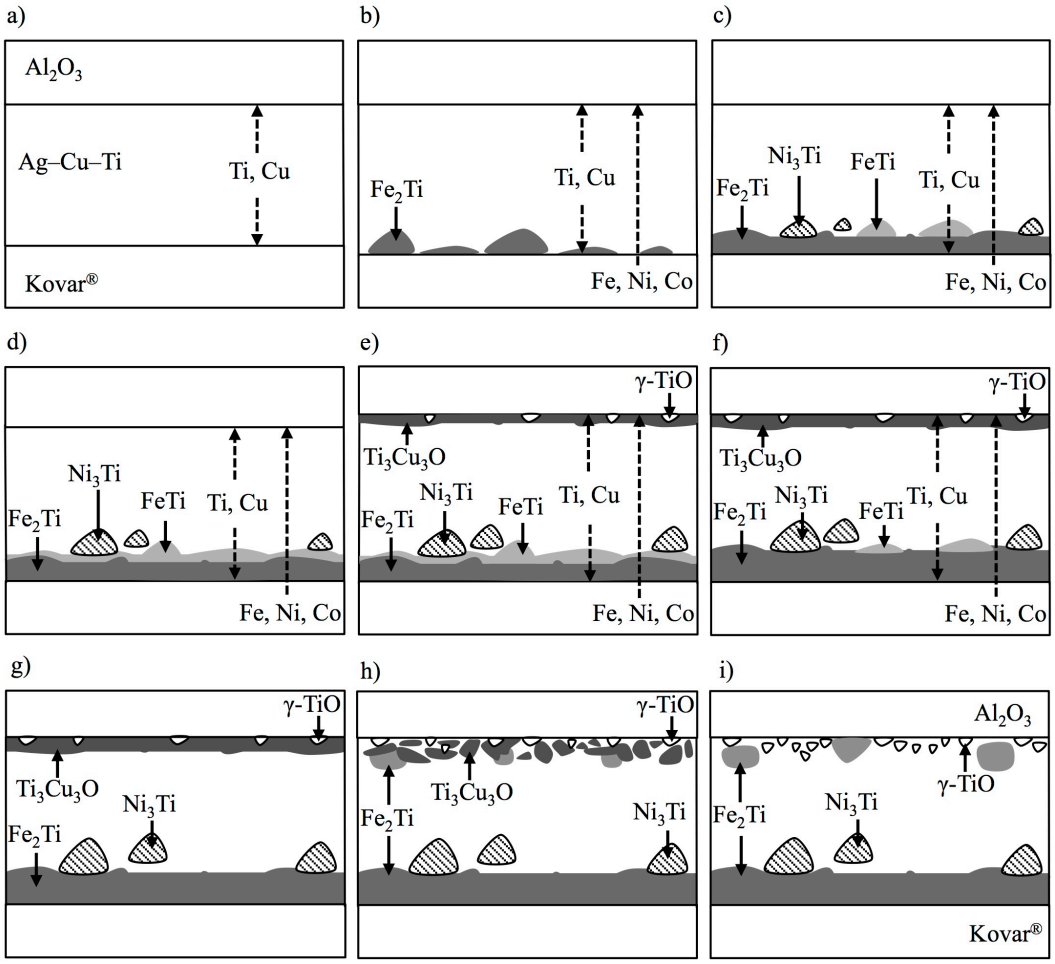

Figure 13. Schematic mechanism for the evolution of the interfacial phases in a 95 wt.% Al_2O_3/Cusil ABA®/Kovar® joint; the Al_2O_3 contains silicon and calcium oxides as secondary phases. Dashed arrows are used to indicate the diffusion of chemical elements and solid arrows are used to label phases. Further details are explained in section 4.1.